



**UNIVERSITY POLITEHNICA OF BUCHAREST**  
**Doctoral School of Materials Science and Engineering**  
DEPARTMENT OF METAL MATERIALS SCIENCE, PHYSICAL  
METALLURGY



**SUMMARY OF THE DOCTORAL THESIS**  
**Fluoride conversion coatings on biodegradable**  
**Mg-Nd-Y-Zn-Zr alloys**

**Author: Eng. PHAM HONG QUAN**

**Scientific coordinator: Univ. Prof. Habil. Dr. Eng. Antoniac Vasile Iulian**

**Bucharest 2022**



**UNIVERSITY POLITEHNICA OF BUCHAREST**  
**Doctoral School of Materials Science and Engineering**  
DEPARTMENT OF METAL MATERIALS SCIENCE, PHYSICAL  
METALLURGY



# **DOCTORAL THESIS**

## **Fluoride conversion coatings on biodegradable Mg-Nd-Y-Zn-Zr alloys**

**Author: Eng. PHAM HONG QUAN**

**Scientific coordinator: Univ.Prof.Habil.Dr.Eng. Antoniac Vasile Iulian**

### **DOCTORAL COMMITTEE**

<b>Chairman</b>	<b>Prof. dr. eng. Augustin Semenescu</b>	<b>University Politehnica of Bucharest</b>
<b>Scientific coordinator</b>	<b>Univ. Prof. Habil. Dr. Eng. Antoniac Vasile Iulian</b>	<b>University Politehnica of Bucharest</b>
<b>Scientific reviewers</b>	<b>Prof. Dr. Ing. Bejinariu Costică</b>	<b>Technical University "Gheorghe Asachi" Iasi</b>
	<b>Prof. Dr. Ing. Buruiană Daniela Laura</b>	<b>Universitatea „Dunarea de Jos” din Galați</b>
	<b>Prof. habil. dr. Eng. Brândușa Ghiban</b>	<b>University Politehnica of Bucharest</b>

**Bucharest 2022**

## Contents

ABSTRACT .....	4
<b>Chapter 1. State of the art on the magnesium alloys for trauma implants .....</b>	<b>5</b>
1.1. Biomaterials for trauma implants .....	5
1.1.1. Non-resorbable biomaterials .....	9
1.1.2. Resorbable biomaterials .....	16
1.2. Magnesium and magnesium alloys as biomaterials .....	18
1.2.1. General aspects on magnesium and magnesium alloys .....	18
1.2.2. Role of alloying elements in magnesium alloys .....	23
1.2.3. Specific magnesium alloys as potential biomaterials .....	28
1.3. Corrosion of magnesium alloys .....	35
1.4. Animal testing and potential clinical applications .....	44
1.5. Coatings on biodegradable magnesium alloys .....	49
<b>Chapter 2. The objectives of the doctoral thesis .....</b>	<b>60</b>
<b>Chapter 3. Materials, methods and equipment used in experimental research .....</b>	<b>62</b>
3.1. Experimental materials .....	62
3.2. Methods used for surface modifications of the experimental materials .....	66
3.3. Experimental methods and equipment used for characterization and testing .....	69
<b>Chapter 4. Characterization and testing of Mg-Nd-Y-Zn-Zr alloys .....</b>	<b>77</b>
4.1. Materials characterization – structural and surface analysis .....	77
4.2. Corrosion resistance .....	84
4.2.1. Electrochemical corrosion .....	84
4.2.2. Corrosion behaviour assessment through immersion tests .....	88
4.3. Mechanical properties by tensile test evaluation .....	94
<b>Chapter 5. Characterization and testing of Mg-Nd-Y-Zn-Zr alloys after different surface treatments .....</b>	<b>99</b>
5.1. Structural evaluation of the surface layers by X-ray Diffraction (XRD) .....	99
5.2. Morphological evaluation of the surface layers by Scanning Electron Microscopy ....	101
5.3. Wettability evaluation of the surface layers by contact angle .....	102
5.4. Corrosion resistance of the experimental samples after different surface treatments .....	105
5.4.1. Electrochemical corrosion behaviour .....	105
5.4.2. Corrosion behaviour assessment through immersion tests .....	110
<b>Chapter 6. Conclusions, personal contributions, and future directions .....</b>	<b>121</b>
6.1. Conclusions .....	121
6.2. Personal contributions .....	126
6.3. Future research directions .....	128
6.4. Dissemination of the results obtained .....	129
List of figures .....	131
List of tables .....	135
List of abbreviations.....	136
Bibliography .....	137

## ABSTRACT

Starting from the fact that magnesium and magnesium-based alloys are viable choices for the production of biodegradable implants due to their excellent biocompatibility and taking into account the fact that their use is still being researched due to the too high dissolution rate, due to the low resistance and ductility, this doctoral thesis aims to investigate two different compositions of the biomaterial Mg-Nd-Y-Zn-Zr, proposing as a teaching element the modification of their surface in three ways, thus resulting in six new types of biomaterials.

The main objective of the doctoral thesis was to obtain and test the viability of six new biodegradable materials, four of which with fluoride conversion coatings on biodegradable Mg-Nd-Y-Zn-Zr alloys and two sandblasted, properly tested to meet the desired requirements in an environment biologically imposed by their use.

To fulfill the main objective of the doctoral thesis, three stages were completed: in the first stage, the original samples were analysed, without influencing the surface, in the second stage, the surface of the investigated alloys was modified by physical-chemical methods. The surface of the first set of samples was modified by treating them with hydrofluoric acid. In the case of the second set of samples, the surface was modified by sandblasting using aluminum. The surface of the third set of samples was initially modified by sandblasting and then treated with hydrofluoric acid, thus suffering 2 surface layers. After that, in the third stage, all samples were investigated by XRD, EDS, and SEM. The degree of wettability was determined by the contact angle method and the corrosion resistance tests were performed and the mechanical properties were evaluated by the tensile test. To observe the biodegradation behavior, the immersion test was made in simulated body fluid for all samples, and the weight loss was calculated. Subsequently, the surface morphology and composition of the corrosion products were examined by SEM and EDS.

Experimental research has revealed that treatment with hydrofluoric acid is a way to improve the bifunctional properties necessary for the analysed magnesium alloys that would be used as orthopedic implants.

In conclusion, the study shows that hydrofluoric acid treatment is an advantageous way to improve the bifunctional properties required for Mg-Nd-Y-Zn-Zr-type Mg alloys to be used as biomaterials for the manufacture of orthopedic implants.

**Keywords:** magnesium-based alloys, biodegradable materials; magnesium coatings; hydrofluoric acid treatment, surface modifications

# **SYNTHETIC PRESENTATION OF THE CHAPTERS OF THE DOCTORAL THESIS**

## **Chapter 1. State of the art on the magnesium alloys for trauma implants**

Biomaterials used for orthopedic implants for osteosynthesis can be of two categories: non-resorbable or resorbable. Biodegradable metals are metals that corrode progressively in the host organism, which respond adequately to the corrosion products, subsequently dissolving in the organism after healing. Therefore, the major component of biodegradable metals is the essential metal elements, which can be absorbed by the body. Biodegradable metals must provide the mechanical support related to supporting the healing process. The major problem is the correlation of the biodegradation rate with the functional necessity imposed on each type of implant.

The use of resorbable materials for the execution of orthopedic implants represents a new direction, with major advantages both for the patient and for the doctor. The purpose of this type of bioresorbable implant is to support the regeneration and healing of tissues, resorbing completely when its purpose is reached, being characterized by the capacity of biodegradation and biocompatibility, the main facility being the elimination of a new subsequent surgical intervention, in order to extract the implant.

Mg and Mg alloys are encouraging biomaterials for producing biodegradable implants because of their excellent biocompatibility. However, the use of Mg alloys is still under research due to significant drawbacks such as high dissolution rate, low strength and ductility. Magnesium-based alloys have become an important class of materials attracting attention thanks to their high potential to be used as temporary implants [1–7]. In order to adapt the properties, some specific alloy systems for biomedical applications are being researched several types of magnesium-based alloys [8].

The characteristics and functionality of Mg-based implants are directly influenced by the fabrication techniques utilized to create them. At the industrial level, casting, powder metallurgy, and additive manufacturing technology based on lasers are the three primary conventional processes used.

The coating processes of magnesium alloys represent modifications of their surface with the aim of preventing direct contact between the magnesium alloy substrate and the human environment, so that corrosion phenomena will be inhibited or delayed, they represent a very attractive way of improving the corrosion resistance of magnesium alloys. In general, coverages can be divided into two classes: conversion coverages and deposited coverages.

## **Chapter 2. The objectives of the doctoral thesis**

The main objective of the doctoral thesis is to obtain and test the viability of six new biodegradable materials, four of which with fluoride conversion coatings on biodegradable Mg-Nd-Y-Zn-Zr alloys and two sandblasted, properly tested to meet the desired requirements in an environment biologically imposed by their use.

In order to fulfill the main objective of the doctoral thesis, three stages were completed:

In the first stage, the original samples were analysed, without influencing the surface. To carry out the second stage, the surface of the investigated alloys was modified by physical-chemical

methods. The surface of the first set of samples was modified by treating them with hydrofluoric acid. In the case of the second set of samples, the surface was modified by sandblasting using aluminium. The surface of the third set of samples was initially modified by sandblasting and then treated with hydrofluoric acid, thus suffering 2 surface layers. For structural characterization, the samples were analyzed by XRD. EDS tests were performed to obtain the elemental composition. To obtain the morphology of the surfaces, images were obtained by SEM. Later, the degree of wettability was determined by the contact angle method and the corrosion resistance tests were performed and the mechanical properties were evaluated by the tensile test.

In order to observe the biodegradation behaviour of the samples treated in the laboratory conditions, after surface modifications, in the next study it was made the immersion test in simulated body fluid for all samples. The testing of the samples consisted of immersing the experimental samples, at a temperature of 37°C, in containers containing sodium chloride at a pH of 7.0. At an interval of 1, 3, 5, 7 and 14 days, the NaCl solution was changed for the samples, they were weighed (after washing and prior drying) and it was calculated the weight loss. Subsequently, the surface morphology and the composition of the corrosion products were examined by SEM and EDS.

## Chapter 3. Materials, methods and equipment used in experimental research

### 3.1. Experimental materials

The materials investigated are MRI 201S – named Sample 1 and MRI 202S – named Sample 2. These materials were supplied by the DSM Company (Beersheva, Israel).

The chemical composition of the the investigated samples is presented in table 3.

**Table 3.** The chemical compositions of the experimental samples

No	Samples	Zn (%)	Zr (%)	Y (%)	Nd (%)	Fe (%)	Si (%)	Ni (%)	Cu (%)	Others each, max (%)	Mg (%)
1	SAMPLE 1	0.3	0.6	2.10	3.2	0.005	0.01	0.001	0.001	0.01	Bal.
2	SAMPLE 2	0.3	0.4	0.21	3.1	0.004	0.01	0.001	0.001	0.01	Bal.

In order to perform experiments to modify the surface of Mg alloys by the sandblasting method, specimens of sample 1 and sample 2 were prepared by going through several stages, namely: cutting, grinding, polishing and cleaning of samples

Eight new experimental samples of two basic magnesium alloys were obtained as follows:

1. original untreated for Sample 1 alloy
2. original untreated for Sample 2 alloy
3. fluoride treated for Sample 1 alloy
4. fluoride treated for Sample 2 alloy
5. the sandblast of the samples Sample 1
6. the sandblast of the samples Sample 2
7. combined treated samples (sandblasted + HF) samples Sample 1
8. combined treated samples (sandblasted + HF) samples Sample 2

The original samples were analysed, without influencing the surface.

For structural characterization, the samples were analysed by Optical Microscopy and XRD. EDS tests were performed to obtain the elemental composition. To obtain the morphology of the surfaces, images were obtained by SEM. Later, the degree of wettability was determined by the contact angle method, the corrosion resistance tests were performed, and the mechanical properties were evaluated by the Tensile Test.

### 3.2. Methods used for surface modifications of the experimental materials

To carry out the second part of the thesis, the surface of the investigated alloys was modified by physical-chemical methods.

The surface of the first set of samples was modified by treating them with hydrofluoric acid. In the case of the second set of samples, the surface was modified by sandblasting using aluminium. The surface of the third set of samples was initially modified by sandblasting and then treated with hydrofluoric acid, thus suffering 2 surface layers.

For structural characterization, the samples were analyzed by XRD. EDS tests were performed to obtain the elemental composition. To obtain the morphology of the surfaces, images were obtained by SEM. Later, the degree of wettability was determined by the contact angle method and the corrosion resistance tests were performed.

### 3.3. Experimental methods and equipment used for characterization and testing

The original samples were analysed, without influencing the surface. For structural characterization, the samples were analysed by Optical Microscopy and XRD. Energy Dispersive X-ray Spectroscopy (EDS) tests were performed to obtain the elemental composition. To obtain the morphology of the surfaces, images were obtained by Scanning Electron Microscopy (SEM). Later, the degree of wettability was determined by the contact angle method, the corrosion resistance tests were performed, and the mechanical properties were evaluated by the Tensile Test.

**Table 3.3.** Methods of characterization of the obtained samples

<b>Laboratory investigations</b>	<b>Characterization method</b>
<b>Chemical characterization</b>	Energy Dispersive X-ray Spectroscopy (EDS)
<b>Structural characterization</b>	Optical microscopy (OM)
	Scanning Electron Microscopy (SEM)
	X-ray Diffraction (XRD)
<b>Physical-Chemical and Mechanical Characterization</b>	Wettability Immersion test Electrochemical corrosion Tensile test

#### **Optical microscopy**

Structural characterization was performed by optical microscopy using an Olympus BX51 microscope.

#### **X-ray Diffraction**

The structural aspects of the experimental samples were determined by using a Panalytical X-Pert PRO Diffractometer.

### **SEM Coupled with EDS**

The elemental composition and the surface morphology of the samples before and after immersion testing were examined under a scanning electron microscope Philips XL 30 ESEM TMP coupled with energy X-ray dispersive spectroscopy system (EDS, EDAX Sapphire Spectrometer).

### **Stereomicroscopy**

A stereomicroscope IOR-MS200X was used to highlight some relief aspects of the surface of the experimental samples after tensile strength.

### **Contact angle**

We used a KRÜSS DSA30 Drop Shape Analysis System. The images were processed by aligning the tangent at the profile of the sessile drop at the point of contact with the surface. All the measurements were made in triplicate and an average value was calculated.

### **Electrochemical tests**

The technique chosen for the determination of corrosion resistance was that of linear polarization at  $37 \pm 0.5^\circ\text{C}$  in NaCl. The corrosion resistance evaluation tests were carried out with a Potentiostat / Galvanostat (PARSTAT 4000 model), and the potentiodynamic curves were acquired with the VersaStudio software [9]. All measurements were achieved according to the ASTM G5-14e1 standard [10].

### **Immersion test**

The testing of the samples consisted of immersing the experimental samples, at a temperature of  $37^\circ\text{C}$ , in containers containing sodium chloride at a pH of 7.0. At an interval of 1, 3, 5, 7 and 14 days, the NaCl solution was changed for the samples and they were weighed (after washing and prior drying). The surface morphology of the experimental samples after immersion testing and the composition of the corrosion products were tested by Sem with EDS.

### **Tensile strength**

The tests were performed on a mechanical testing machine, the INSTRON 3382 model. The main working parameters, which intervened in the tensile tests, were: the test temperature –  $23^\circ\text{C}$  and the moving speed of the mobile crossbar (test speed) – 2 mm/min.

## **Chapter 4. Characterization and testing of Mg-Nd-Y-Zn-Zr alloys**

### **4.1. Materials characterization – structural and surface analysis**

In the first part of the thesis consist in investigation of the the original samples were analysed, without influencing the surface. For structural characterization, the samples were analyzed by Optical Microscopy and XRD. EDS tests were performed to obtain the elemental composition. To obtain the morphology of the surfaces, images were obtained by SEM. Later, the degree of wettability was determined by the contact angle method, the corrosion resistance tests were performed, and the mechanical properties were evaluated by the tensile test.

#### **4.1.1. Optical Microscopy**



It can be observed that the icosahedral phase of the form  $Mg_3(Y)_1(Mg, Zn)_6$  [11] also alloyed with Nd, is present in the solidification mechanisms. This phase contributes substantially to increasing the mechanical characteristics of the material, as well as to those of machinability. Figure 35 shows the optical micrographs corresponding to the Mg-Nd-Y-Zn-Zr alloys - sample 1, at different magnifications. The structure is made up of fine and uniform polyhedral grains of  $\alpha$ -Mg, in which secondary phases are precipitated, with different morphologies, from acicular to globular, the distribution in the grains being uniform, as well as a separate phase at the grain boundary, most likely a multicomponent intermetallic compound.

Figure 36 shows the optical micrographs corresponding to the sample 2, at different magnifications. The structure is made up of fine and uniform polyhedral grains of  $\alpha$ -Mg, in which secondary phases are precipitated, with different morphologies, from acicular to globular, the distribution in the grains being uniform, as well as a separate phase at the grain boundary, most likely a multicomponent intermetallic compound. Eutectic was not identified, which is also to be expected, if we take into account the fact that the alloy has only 0.3% Zn and 0.6% Zr, but 2.1% Y and respectively 3.25 Nd, which it is practical to double the sum of Y+Nd alloying elements compared to the Mg-Nd-Y-Zn-Zr alloys – sample 2.

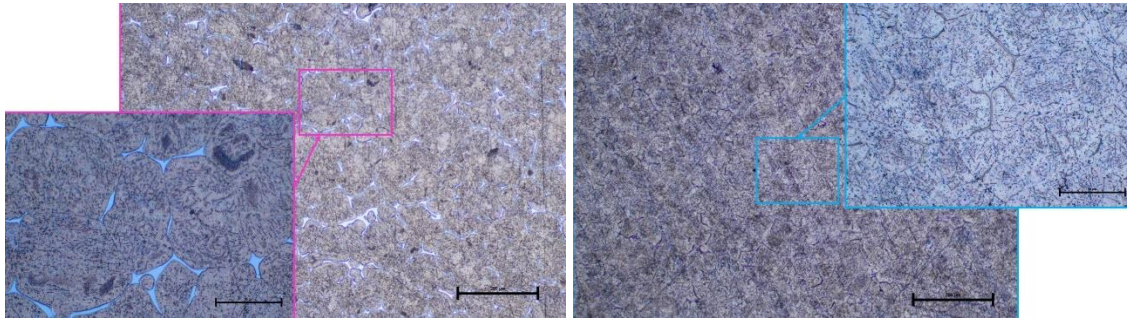


**Figure 35 and 36** The optical micrographs corresponding to the type of alloy Mg-Nd-Y-Zn-Zr alloys corresponding to the chemical composition of both samples

#### 4.1.2. XRD

The XRD spectra obtained on all experimental magnesium alloys samples are shown in Figures 37 and 38. The original magnesium alloys Sample 1 and Sample 2 reveal the presence of magnesium and MgO phases.

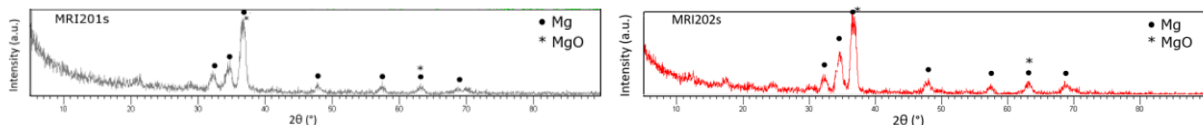


**Figure 37.** XRD diffraction patterns on untreated and treated Sample 1 and 2

#### 4.1.3. SEM-EDS before immersion test

For original magnesium alloys Sample 1 and Sample 2, SEM images show the precipitation of a secondary phase at the grain boundary. A more uniform distribution of the secondary phase at the grain boundary is observed in the case of Sample 2 alloy. It is observed that the treatment of both experimental alloy samples (Sample 1 and Sample 2) with HF conduct to a similar smoother

surface without changing the morphology of the substrate. The layer of  $MgF_2$  formed at the surface is very thin, that permit a clear visualization of the grain boundaries.

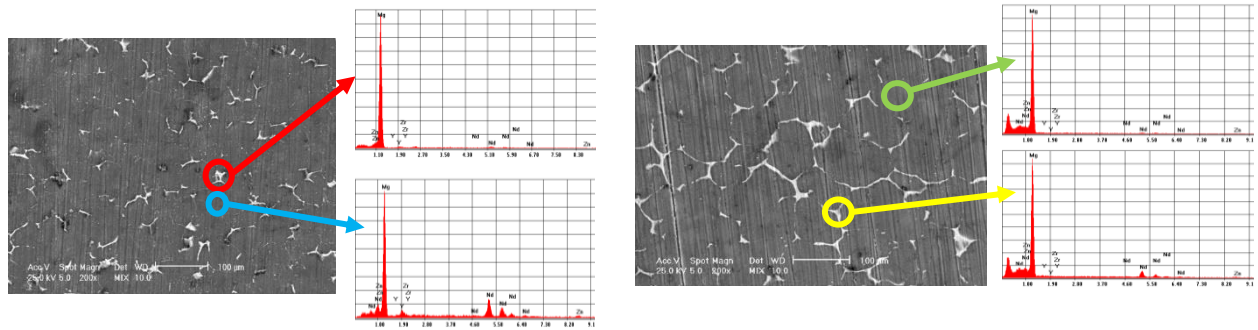


**Figure 39.** SEM-EDX images obtained after the surface analysis of the untreated Sample 1, highlighting the compounds at the grain boundary (red) and the surface composition (blue) and the compounds at the grain boundary (yellow) and the surface composition (green) (sample 2)

#### 4.1.4. Contact angle.

As we can see in figures above the contact angle decreases in the case of all samples with HF treated surface, from  $61^\circ$  to  $20^\circ$  for Sample 1 alloy and from  $55^\circ$  to  $16^\circ$  for Sample 2 alloy [63]. Results obtained for sandblasted samples shown that the hydrophobicity have increased and lose their hydrophilic character.

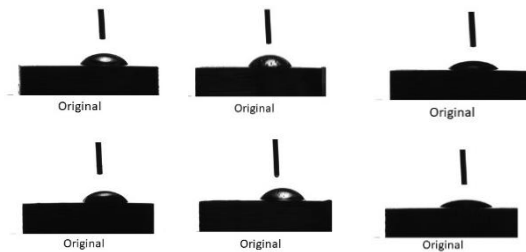


**Figure 41.** The contact angles measurements for each type of Sample 1 sample with three liquids (diiodomethane, ethylene glycol and water)

**Figure 42.** The contact angles measurements for each type of Sample 2 sample with three liquids (diiodomethane, ethylene glycol and water)

## 4.2. Corrosion resistance

### 4.2.1. Electrochemical corrosion

Magnesium alloys are known to degrade in aqueous media through electrochemical corrosion reactions that produce magnesium hydroxide and hydrogen [3]. Some studies demonstrate that in the case of corrosion testing by electrochemical methods or immersion tests of some biodegradable magnesium alloys after fluoride treatment, the HF concentration is important, because a more uniform, dense and thick coating layer was obtained when a higher HF concentration (40%) was used [36,37,40].

In the Figure 43 are presented the open circuit potential curves and in Figure 32 the Tafel plots of magnesium alloys in NaCl solution.

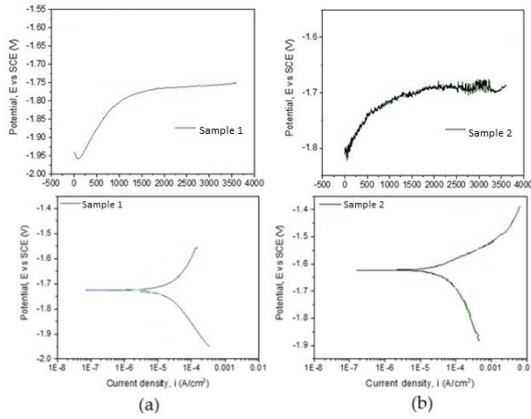
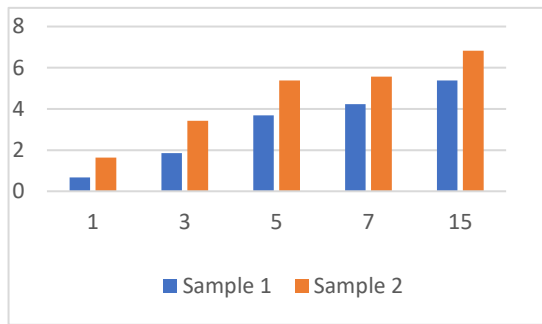


**Figure 43** The open circuit potential curves of magnesium alloys: Sample 1(a), Sample 2(b).

**Figure 44** The Tafel plots of magnesium alloys: Sample 1 and Sample 2.

#### 4.1.6. Corrosion behaviour assessment through immersion tests Weight loss determination

The evolution of the degradation rate assessed by determining weight loss is presented in figure



33.

**Figure 45.** Weight loss of untreated and treated Sample 1 and Sample 2 samples after 1, 3, 5, 7 and 14 days of immersion in NaCl solution

The degradation rate of untreated Sample 1 and Sample 2 alloys is higher due to the existence of a high concentration of  $\text{Cl}^-$  ions in the test medium. Corrosion of Sample 1 and Sample 2 magnesium

alloys is a redox process of magnesium oxidation, a process coupled with the reduction and formation of hydrogen both from hydrogen ions and/or the hydrogen atom in the water molecule [46, 47]. The  $\text{Cl}^-$  ions present in the test environment transform the  $\text{Mg}(\text{OH})_2$  layer formed at the surface (according the equation 3.8) into  $\text{MgCl}_2$ , a soluble precipitate in solution [48, 49].

This process causes an increase in hydroxide ions ( $\text{OH}^-$ ) nearby the surface of the sample leading to an increase in the pH of the solution. The corrosion process takes place until the corrosion layer ( $\text{Mg}(\text{OH})_2$ ) that forms in these regions, reaches a saturation point, at a pH value of at least 10.4.

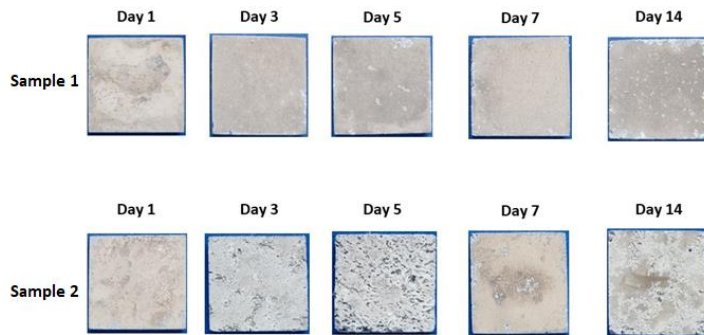


**Figure 46.** Macroscopic aspect of the untreated experimental samples after 1, 3, 5, 7 and 14 days of immersion in sodium chloride solution

By analysing the two initial Mg alloys, it can be seen that the samples 2 is more degraded. This is probably due to the higher amount of Y in the

chemical composition of the Mg alloy. This element gives a higher homogeneity of the grains in the microstructure.

#### 4.1.7. SEM-EDS after the immersion test

In the SEM images on Sample 1, investigated after 5 days of immersion (Figure 47), it can be observed the formation at the surface of dense spherical corrosion products. After immersion in NaCl for 14 days, a layer of corrosion products with a large number of clusters appeared on the samples surfaces. The presence of this layer at 14 days of immersion suggests that the material exchange process is fast but without the formation of cracks on the samples surface that would produce an aggressive corrosion process.

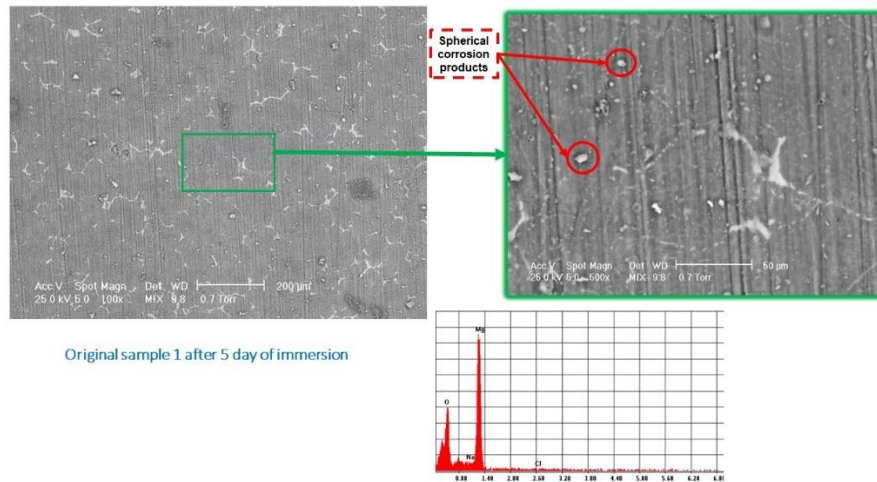


**Figure 47.** Surface morphologies of the original experimental sample Sample 1 after 5 days of immersion in sodium chloride solution – with the highlighting of the spherical corrosion products

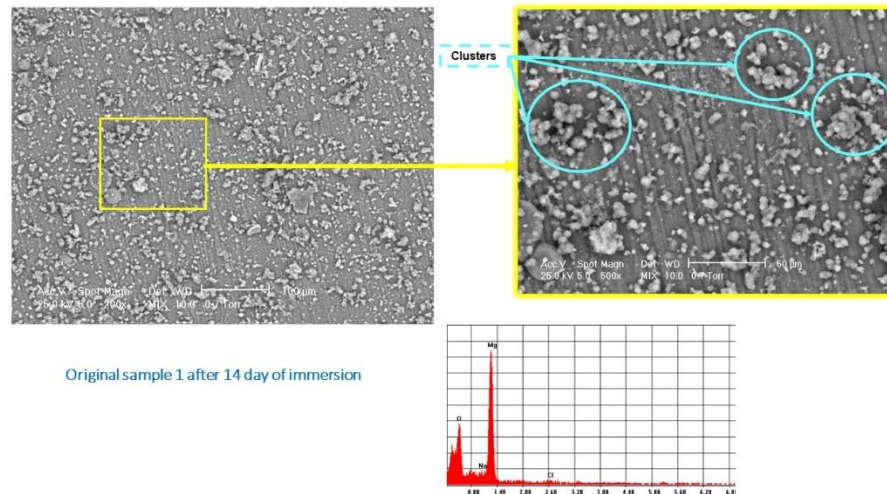


**Figure 48.** Surface morphologies of the original experimental sample Sample 1 after 14 days of immersion in sodium chloride solution – with the highlighting of the clusters

For Sample 2 the process is more intense after the obtaining of a dense layer of corrosion products is visible after 7 days of immersion in NaCl.

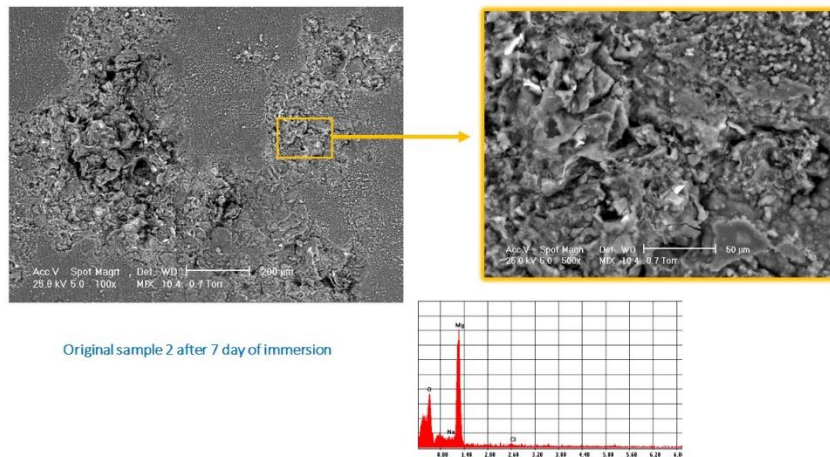


**Figure 49.** Surface morphologies of the original experimental sample Sample 2 after 7 days of immersion in sodium chloride solution – with the highlighting of the corrosion products

### 4.3. Mechanical properties by tensile test evaluation

#### Analysis of the shape and appearance of the specimen after breaking

The fracture of a material can be ductile, brittle or mixed. In the case of ductile fracture, the material allows strong plastic deformations, and in the case of brittle fracture, the crack propagates suddenly, there is no global deformation of an area of the material, but only a local microdeformation on the fracture surface.

In the case of tensile specimens, brittle fracture produces a separation section normal to the axis. This type of rupture occurs suddenly, without any prior manifestation, and the rupture section has a grainy structure. Test pieces made of very plastic materials (gold, lead) get a big neck, and at the time of breaking the section can even reach a point.

Materials with medium ductility have, before breaking, a rather pronounced necking. In these, the break starts from the center of the sample section and propagates along the directions of the maximum tangential stresses (at  $45^\circ$ ), the appearance of the break surface being called "concrater".

In the case of samples 1 and 2, the characteristics of the materials are highlighted both by the sudden break, with a prior manifestation of reduced dimensions, and by the presence of the grainy structure of the material in the break section (according to the figure 51).

The diagrams show the nature of the materials and the maximum stress that each of the two analysed materials can withstand, respectively a maximum stress of 203,914 MPa for sample 1 and a maximum stress of 187,228 MPa for sample 2.

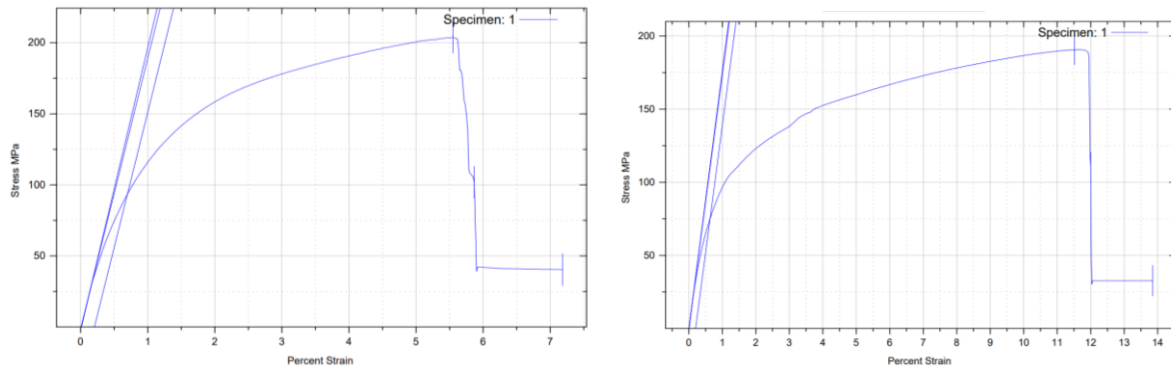


**Figure 52** The tensile stress-strain diagrams highlighting the mechanical properties of the alloys investigated.

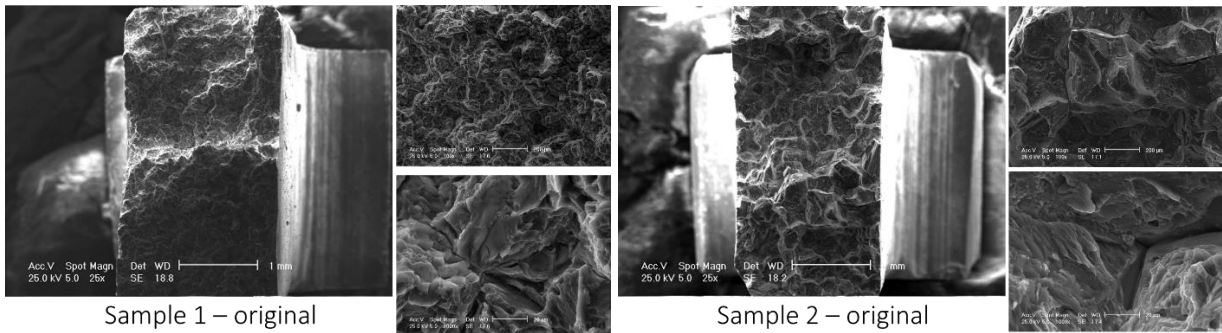


**Figure 53.** SEM images obtained after tensile strength testing for original untreated for bought samples.

## Chapter 5. Characterization and testing of biodegradable Mg-Nd-Y-Zn-Zr alloys after different surface treatments

To carry out the second part of the experimental program, the surface of the investigated alloys was modified by physical-chemical methods. It resulted three new types of Mg-Nd-Y-Zn-Zr alloys.

The surface of the first set of samples was modified by treating them with hydrofluoric acid (samples named Sample 1 – H and Sample 2 – H).

In the case of the second set of samples, the surface was modified by sandblasting using aluminium (samples named Sample 1 – S and Sample 2 – S).

The surface of the third set of samples was initially modified by sandblasting and then treated with hydrofluoric acid, thus suffering 2 surface layers (samples named Sample 1 – SH and Sample 2 – SH).

For structural characterization, the samples were analyzed by XRD. EDS tests were performed to obtain the elemental composition. To obtain the morphology of the surfaces, images were obtained by SEM.

Later, the degree of wettability was determined by the contact angle method and the corrosion resistance tests were performed and the mechanical properties were evaluated by the tensile test.

## 5.1. Structural evaluation of the surface layers by X-ray Diffraction (XRD)

The XRD spectra obtained on all experimental magnesium alloys samples are shown in Figures 54 and 55. Compared to the original magnesium alloys Sample 1 and Sample 2 which revealed the presence of magnesium and MgO phases in HF-treated alloys (Sample 1-H, Sample 1-SH, Sample 2-H, Sample 2-SH) the presence of MgF<sub>2</sub> in the conversion layer is observed.

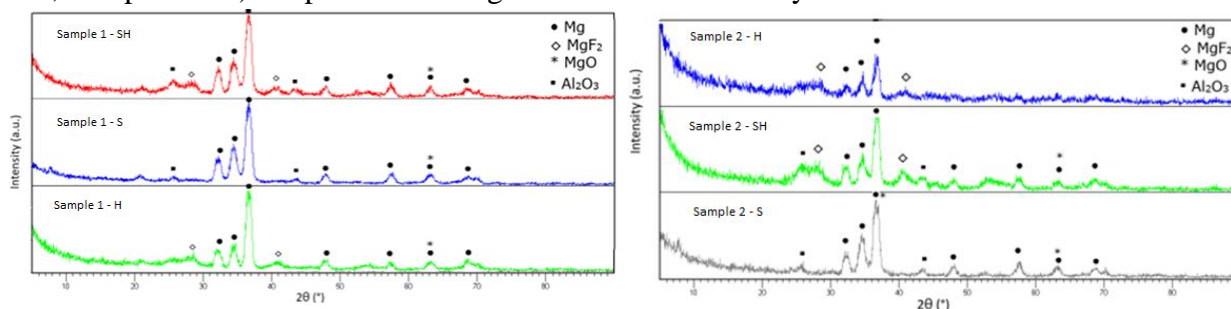


**Figure 54.** XRD diffraction patterns on treated Sample 1 and 2

In XRD patterns for sandblasted treated surface samples, Al<sub>2</sub>O<sub>3</sub> phase were detected, indicating residual particles after the sandblasting treatment. In all XRD patterns for treated magnesium alloys the Mg phase is observed, phase from the substrate which is present because of the thin layer formed at the surface.

## 5.2. Morphological evaluation of the surface layers by Scanning Electron Microscopy

The SEM images obtained after the surface analysis of the three types treated samples (with HF, sandblasted and initially modified by sandblasting and then treated with hydrofluoric acid), are shown in figures below.

A more uniform distribution of the secondary phase at the grain boundary is observed in the case of Sample 2 alloy. It is observed that the treatment of both experimental alloy samples (Sample 1 and Sample 2) with HF conduct to a similar smoother surface without changing the morphology of the substrate. The layer of MgF<sub>2</sub> formed at the surface is very thin, that permit a clear visualization of the grain boundaries.

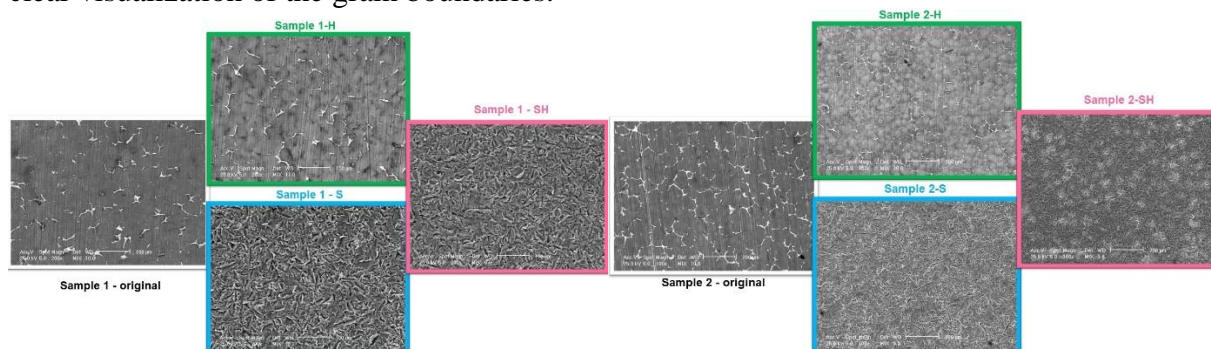


**Figure 56** Sample 1 – SEM images for the original and treated surfaces

In the case of sandblasted samples, SEM image exhibit for the two alloys studied many deep cavities over the whole surface. We notice that the roughness of the samples surface increased with the sandblasting process.

As a result, the surface where there is contact with the corrosion medium increases, which generates a decrease of the corrosion resistance of the samples in comparison to the samples treated with hydrofluoric acid.

### 5.3. Wettability evaluation of the surface layers by contact angle.

Considering that a small contact angle so a hydrophilic surface, will improve cell adhesion while a hydrophobic surface can affect cell adhesion and protein denaturation, leading to the rejection of implantable material, it was teste also the contact angle for the samples threated physic-chemical.

The obtained results are presented in table 9 and the corresponding images in Figure 58 and 59.

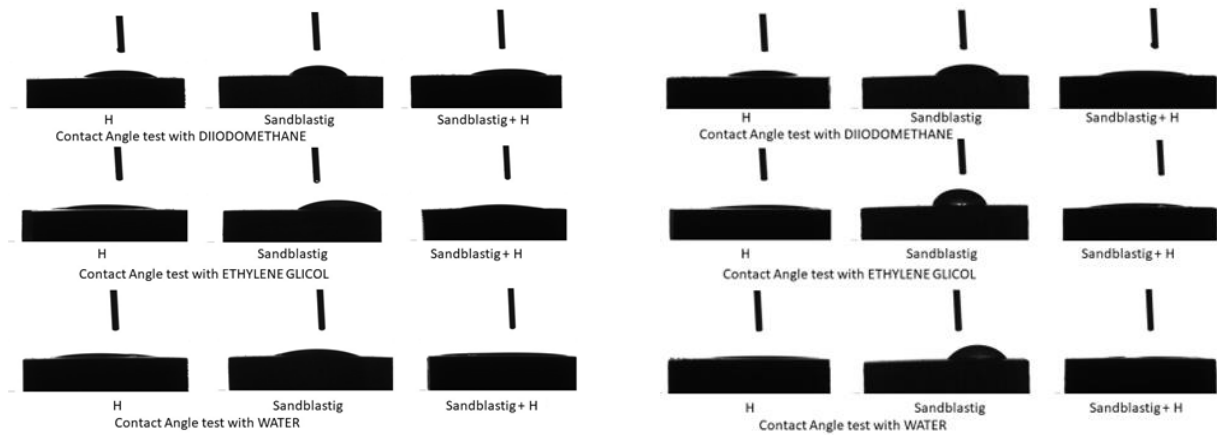


**Figure 58.** The contact angles measurements for samples 1 and 2 threated physic-chemical with three liquids (diiodomethane, ethylene glycol and water)

As we can see in figures above the contact angle decreases in the case of all samples with HF treated surface, from  $61^\circ$  to  $20^\circ$  for Sample 1 alloy and from  $55^\circ$  to  $16^\circ$  for Sample 2 alloy [63]. Results obtained for sandblasted samples shown that the hydrophobicity have increased and lose their hydrophilic character.

## 5.4. Corrosion resistance of the experimental samples after different surface treatments

### 5.4.1. Electrochemical corrosion behaviour

Some studies demonstrate that in the case of corrosion testing by electrochemical methods or immersion tests of some biodegradable magnesium alloys after fluoride treatment, the HF concentration is important, because a more uniform, dense and thick coating layer was obtained when a higher HF concentration (40%) was used [36,37,40]. Electrochemical tests prove that fluoride layer determines an increase of the corrosion resistance, but several corrosion dots are present. Ren et al. [56] studied calcium phosphate glass/MgF<sub>2</sub> double layered composite coating on AZ31 magnesium alloy.

It was concluded after microstructural analysis and classical corrosion tests that the corrosion current density is reduced at  $0.6\mu\text{A}/\text{cm}^2$  and the charge transfer resistance increases with two magnitude order. The pH of the double coated sample decreases, and a large adhesion strength was observed. Immersion tests prove that the CaP glass/MgF<sub>2</sub> composite coating provides a high corrosion protection for the Mg substrate, and it is very suitable for using for implants, because it is biodegradable. Reza Bakhsheshi-Rad et al. [57] has applied a fluoride treatment in the case of a



Mg-Ca binary alloy, but on a Mg-0.5Ca alloy and conclude that Mg-0.5Ca treated with 40% HF presents a low degradation kinetics and a high biocompatibility.

In the Figure 31 are presented the comparative open circuit potential curves and in Figure 32 the comparative Tafel plots of magnesium alloys in NaCl solution.

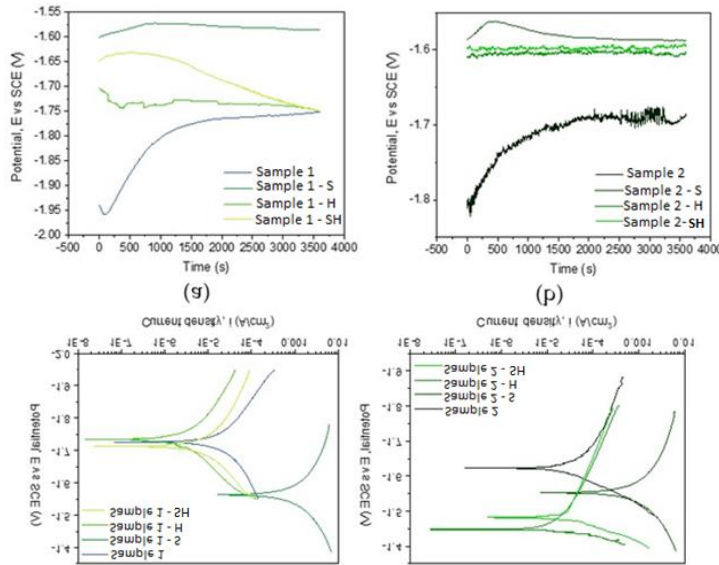


**Figure 60** The open circuit potential curves of magnesium alloys: Sample 1 alloy (a), Sample 2 alloy (b).

**Figure 61** The Tafel plots of magnesium alloys: Sample 1 alloy (a), Sample 2 alloy (b).

According to the obtained results presented in Table 10 it can be observed that after sandblasted the alloys have a poor corrosion resistance and the treatment with HF have enhanced the electrochemical

behaviour of the investigated magnesium alloys samples regardless of surface treatment.

The electrochemical results reveal that after chemical treatment with HF solution of both investigated magnesium alloys, they exhibit the lowest corrosion current density, highest polarization resistance, and a corrosion resistance of almost 10 times higher for Sample 1-H alloy, and almost four times higher for Sample 2-H alloy compared with untreated magnesium alloys. In relation to untreated alloys, for the Sample 1-S and Sample 2-S samples, the electrochemical results revealed the degradation of the surface layer and a decrease of the corrosion resistance caused by the initial sandblasting of the samples. Furthermore, after the immersion test the degradation rates for both sandblasted samples are significantly increased mainly due to the high surface roughness and deep cavities formed at the surfaces, which increase substrate activity.

#### 4.2.5. Corrosion behaviour assessment through immersion tests

##### Weight loss determination

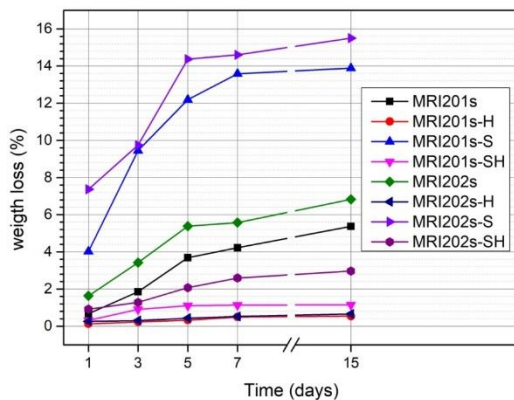


**Figure 62.** Weight loss of untreated and treated Sample 1 and Sample 2 after 1, 3, 5, 7 and 14 days of immersion in NaCl solution

The evolution of the degradation rate assessed by determining weight loss is presented in figure 62. In the case of both experimental alloys (Sample 1 and Sample 2), the treatment with HF induces a reduction of the degradation process even the samples were sandblasted previously or not.

The weight loss of Sample 1-H and Sample 2-H (HF treated) and Sample 1-SH and Sample 2-SH (sandblasted and treated with HF) respectively was lower than in the case of untreated samples for the entire stage. This is due to the  $MgF_2$  layer formed on the samples which acts like an inhibitor and protects them from corrosion.

The results obtained for sandblasted samples indicate a significant increase in weight loss compared to the original samples. In general, the alloys degradation rate increased with a higher surface roughness [50-52]. Sandblasting of the magnesium alloys surface induces a high dislocation density and the formation of deep cavities, which increase substrate activity [63].

The surface morphologies of the experimental samples after 1, 3, 5, 7 and 14 days of immersion in sodium chloride solution are shown in Figure 33.

**Table 12** - Weight loss measurements values

Sample 1 - Original	$m_0$ (g)	1 day		3 days		5 days		7 days		14 days	
		$M_1$ (g)	pH	$M_3$ (g)	pH	$M_5$ (g)	pH	$M_7$ (g)	pH	$M_{14}$ (g)	pH
$M_{III-1i}$	2.0433	2.0459	10.50								
$M_{III-3i}$	2.1312			2.1362	10.15						
$M_{III-5i}$	2.0462					2.0483	10.50				
$M_{III-7i}$	2.0546							2.0580	10.56		
$M_{III-14i}$	2.0113									2.0117	10.46

**Table 13** - Weight loss measurements values

Sample 2 - Original	$m_0$ (g)	1 day		3 days		5 days		7 days		14 days	
		$M_1$ (g)	pH	$M_3$ (g)	pH	$M_5$ (g)	pH	$M_7$ (g)	pH	$M_{14}$ (g)	pH
$M_{IV-1i}$	1.7834	1.7766	10.49								
$M_{IV-3i}$	1.7238			1.7169	10.55						
$M_{IV-5i}$	1.8544					1.7555	10.48				
$M_{IV-7i}$	1.7197							1.7128	10.47		
$M_{IV-14i}$	1.7440									1.7360	10.43

By analysing the two initial Mg alloys, it can be seen that the samples 2 is more degraded. This is probably due to the higher amount of Y in the chemical composition of this alloy, which gives a higher homogeneity of the grains in the microstructure.

The difference between the behaviour of the two alloys is maintained in the case of samples treated with HF, but is equalized after the application of the blasting treatment or after blasting and treatment with HF.

Regarding the surface modification treatments applied on the initial alloys, it is obvious that the surface sandblasting treatment leads to a more accentuated degradation of the sandblasted samples, regardless of the composition of the alloy. At the same time, the surface has a rougher topography and favours the biomaterial-tissue interaction. This positive effect induced by blasting is also maintained in the case of experimental samples that were treated with HF after blasting, but slightly attenuated.

Macroscopic investigations of the surface of the experimental samples after the immersion test demonstrate that the experimental samples sandblasted and subsequently treated with HF have the best surface properties in terms of biomaterial-tissue interaction.

### SEM-EDS after the immersion test

The SEM images obtained after the immersion test of all samples (original, treated with HF, sandblasted, and initially modified by sandblasting and then treated with hydrofluoric acid), are shown in figures below.

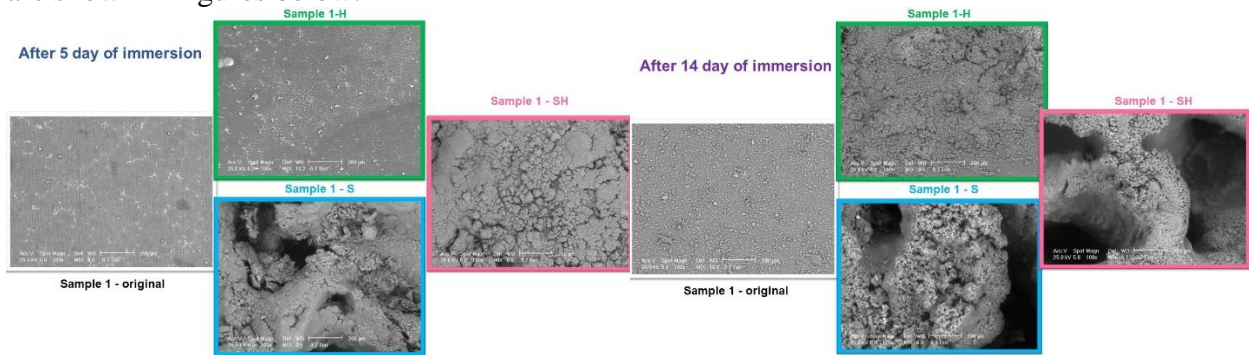


**Figure 66** SEM images aspect of the experimental samples 1 after 5 days of immersion in sodium chloride solution and after 14 days (right)

It is notice that the treatment of all samples with hydrofluoric acid conduct to a similar smoother surface without changing the morphology of the substrate. It is notice a very thin layer of  $MgF_2$  at the surface, layer that allows the observation of very well-defined grains.

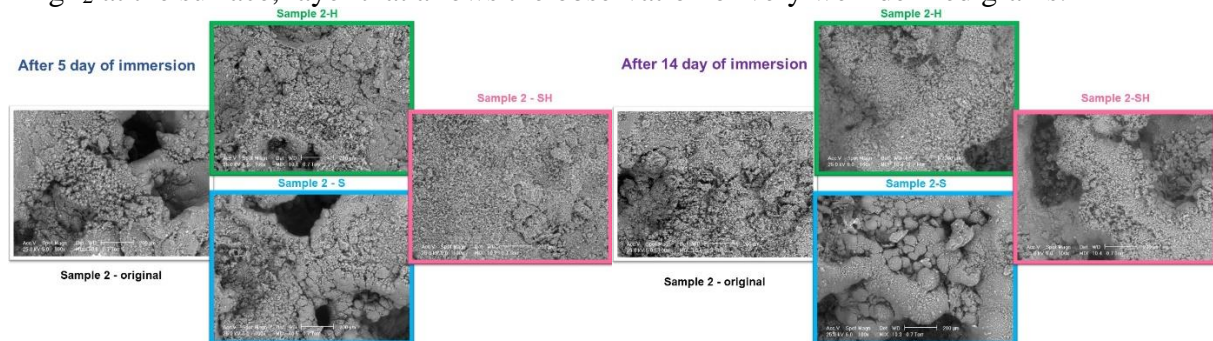


**Figure 68** SEM images aspect of the experimental samples 2 after 5 days of immersion in sodium chloride solution

In the case of all sandblasted samples, both alloys exhibit a lot of deep cavities all over the surface. Obviously, the roughness of the samples surface increased with the sandblasting process. For the sandblasted samples (S-samples – highlighted with blue), the contact surface with the SBF solution increases, implicitly generating a decrease in their corrosion resistance compared to the samples treated with hydrofluoric acid (highlighted with green).

The relatively smooth surface of the hydrofluoric acid-treated samples suggests that the chemical conversion layer of magnesium fluoride is denser than that of the untreated and sandblasted samples, which explains the better corrosion resistance. After 5 days of immersion in NaCl, the presence of corrosion cracks is not observed on the surface of the HF-treated samples, while in the case of sandblasted samples relatively small cracks appear which indicates a more intense corrosion process.

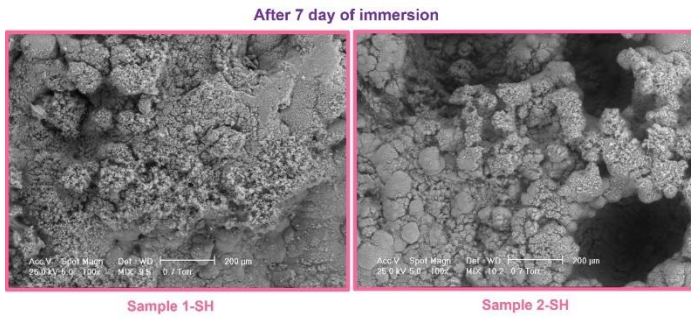


**Figure 70** SEM images aspect of the sandblasted with HF-treated samples 1 and 2 after 7 days of immersion in sodium chloride solution

The sandblasted sample surfaces become uneven with coarse cluster corrosion products. The formation of corrosion cracks is observed also in the case of sandblasted with HF-treated

samples at 5 and 7 days of immersion in NaCl.

## Chapter 6. Conclusions, personal contributions, and future directions

### 6.1. Conclusions

The work with the title “Fluoride conversion coatings on biodegradable Mg-Nd-Y-Zn-Zr alloys” begins with the analysis of the current state of scientific research regarding obtaining new biodegradable magnesium alloys with modified surfaces accordingly to meet the functional requirements of biodegradation in a biological environment imposed by their use in the temporary orthopaedic implants execution.

Theoretical and experimental research were channelled in such a way as to generate major contributions such as:

1. Contributions regarding the opportunity to approach the theme in the content of the research undertaken on a global and national level regarding the biodegradable magnesium alloys with modified surfaces used for temporary orthopedic implants execution.
2. Contributions concerning the establishment of the experimental program and research protocols in accordance with the standards in force and the requests of the European Union.
3. Contributions concerning the transition from theory to the realization and modification of the characteristics of biodegradable magnesium alloys.
4. Contributions regarding the new magnesium alloys with modified surfaces.
5. The theoretical synthesis part includes some original contributions of the author of the doctoral thesis consisting of the integration of the studied problem in the wider framework of knowledge in the field of medical engineering.

The results proven that the original - untreated samples were significantly influenced by SBF, while the hydrofluoric acid-treated samples showed better corrosion resistance. Fluoride conversion coatings on biodegradable Mg-Nd-Y-Zn-Zr alloys by immersion in hydrofluoric acid produces a more uniform, smooth surface, without important changes in the morphology of the substrate, which generates a better protection of the substrate.

We also investigated the effect of the sandblasting treatment of both Mg-Nd-Y-Zn-Zr type alloys using alumina particles, on the degradation behavior in SBF solution.

In the specialized literature it is specified that a more hydrophilic surface, with a smaller contact angle, shows a better adhesion, an increased wettability and a higher free energy of the solid surface [63]. Considering the fact that the alloys investigated in this doctoral thesis are addressed to the orthopedic field, especially for the biomaterials used in osteosynthesis, they must present such characteristics precisely to improve cell adhesion. On the contrary, a hydrophobic surface does not stimulate cell adhesion and leads to the denaturation of proteins, generating possible failures of the operations through the rejection of the material by the body [63]. The obtained results show that both the samples whose surface was treated with hydrofluoric acid (sample H) and the samples that were first sandblasted and later treated with hydrofluoric acid (samples SH) showed a low contact

angle and a more hydrophilic character, while the samples that were only sandblasted with aluminum (Samples S) lost their hydrophilicity, increasing their hydrophobicity [63].

The characteristics of the layers generated on the surface of biodegradable Mg-Nd-Y-Zn-Zr alloys significantly influence their corrosion behavior.

In conclusion:

- treating the biodegradable Mg-Nd-Y-Zn-Zr alloy with hydrofluoric acid positively influences the corrosion process, offering good protection against the environment in which they were immersed
- aluminum sandblasting of a biodegradable alloy of the Mg-Nd-Y-Zn-Zr type negatively influences the corrosion process
- all investigated samples had a more accelerated weight loss in the first 5 days, after which it decreased in intensity. Which means that after these first days, a stable layer of  $Mg(OH)_2$  is formed on the surface of the biomaterials.
- HF treatment is a beneficial way to improve the functional properties to be used as biomaterials for the manufacture of osteosynthesis implants [63]
- to obtain a better interaction between the magnesium alloys and the surrounding tissue, we consider that sandblasting with aluminum followed by treatment with hydrofluoric acid of biodegradable alloys of the Mg-Nd-Y-Zn-Zr type allows obtaining optimal surface properties [63].

As a result of the electrochemical corrosion behavior tests, it was found that the samples covered with hydrofluoric acid solution - for both alloys of the Mg-Nd-Y-Zn-Zr type showed the lowest corrosion current density, simultaneously with the higher polarization resistance. Also, the alloys of the sample 1-H type generated a 9 times higher corrosion resistance, while those of the sample 2-H type also generated a 4 times higher corrosion resistance compared to the original magnesium alloys .

For the sandblasted Mg-Nd-Y-Zn-Zr type alloy samples, the electrochemical tests revealed the degradation of the surface layer and implicitly the decrease in corrosion resistance due to this type of coating. At the same time, the immersion tests showed significant increases in degradation rates, generally due to the roughness of the surface and the cavities formed on the surface of the sandblasted samples, which generate an increase in the activity of the substrate.

Surface wetting has a significant role in the biocompatibility of biomaterials. This is quantified by determining the contact angle values. According to specialized literature, on rough surfaces - such as sandblasted samples - the drop of liquid will not adhere to the surface.

It is also known that a more hydrophilic surface, with a smaller contact angle, reflects good adhesiveness, good wettability, and higher solid surface free energy. Thus, if we talk about osseointegration, a small contact angle, so a hydrophilic surface, will improve cell adhesion while a hydrophobic surface can affect cell adhesion and protein denaturation, leading to the rejection of implantable material. Chengyu Xu et al. [58] showed that surface induce different kinds of cell responses. Fibroblasts prefer smoother surfaces, epithelial cells attached only to the smoothest surfaces while osteoblast cells prefer rougher surface.

According to specialized literature [54, 55], the corrosion resistance of a material exists when all the following are met:

- a more electropositive corrosion potential ( $E_{corr}$ ),
- a low density of the corrosion current ( $i_{corr}$ ) and
- a higher bias resistance ( $R_p$ ).

After the corrosion tests, both samples treated with hydrofluoric acid recorded the lowest  $i_{corr}$  (Sample1-H where  $i_{corr}= 4.203 \mu A/cm^2$  and Sample2-H where  $i_{corr}= 14.87 \mu A/cm^2$ ) but where the  $R_p$  value is the higher (Sample1-H where  $R_p = 8.997 k\Omega \times cm^2$  and Sample 2-H where  $R_p=0.727 k\Omega \times cm^2$ ).

The results of the corrosion tests lead to the conclusion that:

- Sandblasting both samples of the studied alloys of the Mg-Nd-Y-Zn-Zr type led to a decrease in corrosion resistance;
- Covering the samples with hydrofluoric acid of both investigated alloys of the Mg-Nd-Y-Zn-Zr type generated the lowest corrosion current density.
- Covering the samples with hydrofluoric acid of both investigated alloys of the Mg-Nd-Y-Zn-Zr type generated the highest polarization resistance.
- Covering the samples with hydrofluoric acid after previous sandblasting, corrosion resistance is greatly improved for both alloys of the Mg-Nd-Y-Zn-Zr type.

The formation of the thin layer of MgF<sub>2</sub> on the surfaces of the Mg-Nd-Y-Zn-Zr type alloys that were only immersed in hydrofluoric acid, but also on the surface of the Mg-Nd-Y-Zn-Zr type alloys that were initially immersed in acid hydrofluoric and subsequently sandblasted led to a decrease in the corrosion rate, the best values being obtained for Sample 1-H where CR= 0.094 mm/a and Sample 1-SH, CR = 0.342 mm/year.

Both the stability of the MgF<sub>2</sub> thin film, as well as the porosity, chemical composition and uniformity generate an important influence on the corrosion behavior of all samples investigated.

Thus, for both samples of Mg-Nd-Y-Zn-Zr alloys, coating with hydrofluoric acid improved the corrosion resistance, reducing the corrosion process, while sandblasting did not generate this objective.

It is also observed that the chemical composition of the investigated Mg-Nd-Y-Zn-Zr type alloys does not significantly influence the degradation process. Thus, all the samples - regardless of the coatings suffered - had a similar evolution.

The weight loss of all the samples is more accelerated in the first five days, after which the intensity of the process is greatly reduced, which means that the stable and protective layer of Mg(OH)<sub>2</sub> is formed on the surface.

Also, the SEM investigations revealed the fact that, after 14 days of immersion in the NaCl solution, both samples treated in hydrofluoric acid showed the formation of a layer of agglomerated corrosion products (clusters), but also a dense layer of MgCl<sub>2</sub> conversion products, while the samples that were only sandblasted but also those that were previously sandblasted and later treated with hydrofluoric acid showed corrosion cracks.

In conclusion, our study reveals that - hydrofluoric acid treatment is a useful way to improve the functional properties to be used as biomaterials for Mg-Nd-Y-Zn-Zr-type magnesium alloys to be used as biomaterials for the manufacture of orthopedic implants.

## 6.2. Personal contributions

Original contributions and most significant results are:

1. A complex synthesis of the scientific documentation led to many new results and interpretations regarding the opportunity to approach the theme in the content of the research undertaken on a global and national level regarding the biodegradable magnesium alloys with modified surfaces used for temporary orthopedic implants execution .

2. The synthesis from the specialized literature corroborated with the experimental results obtained following the work protocol allowed the formulation of original conclusions regarding the notions of coatings, biocompatibility and biofunctionality.

3. New experimental samples of two basic magnesium alloys were obtained as follows:

- original untreated for Sample 1 alloy
- fluoride treated for Sample 1 alloy
- the sandblast of the samples Sample 1

- combined treated samples (sandblasted + HF) samples Sample 1 and original untreated for Sample 2 alloy
  - fluoride treated for Sample 2 alloy
  - the sandblast of the samples Sample 2
  - combined treated samples (sandblasted + HF) samples Sample 1
4. For structural characterization, the samples were analyzed by Optical Microscopy and XRD.
  5. EDS tests were performed to obtain the elemental composition.
  6. To obtain the morphology of the surfaces, images were obtained SEM.
  7. The degree of wettability was established by the contact angle method.
  8. The corrosion resistance tests were carried out.
  9. A study of the degradation of the samples in simulated physiological environment was carried out.
  10. The mechanical properties were evaluated by the tensile test.

It is mentioned that the experimental part was carried out mainly within the Faculty of Materials Science and Engineering, Department of Materials Science and Physical Metallurgy, but experimental determinations were also carried out in other laboratories from University Polytechnic of Bucharest.

Without pretending to have covered all the existing studies in the current specialized literature in the field of biodegradable magnesium alloys with medical applicability, the work makes a modest theoretical and practical contribution, while also opening new perspectives for future research in this field and beyond.

### **6.3. Future research directions**

Future research will focus on determining biocompatibility both in vitro on cell lines and in vivo in an animal model and by studying the chemical products released from the corrosion of Mg-Nd-Y-Zn-Zr type materials to establish their effects on the human body.

## 6.4. Dissemination of the results obtained

### Articles:

**1. First author article** - *Fluoride Treatment and In Vitro Corrosion Behavior of Mg-Nd-Y-Zn-Zr Alloys Type / revista MATERIALS (Q1)* - <https://www.webofscience.com/wos/woscc/full-record/WOS:000757583600001>, **Quan, PH**; Antoniac, I; Miculescu, F; Antoniac, A; Manescu, V; Robu, A; Bitu, AI; Miculescu, M; Saceleanu, A; Bodog, AD; Saceleanu, V, *15*, 2, 266, **DOI10.3390/ma15020566**

**2. First author article** - *Potential of Biodegradable Magnesium Alloys for Medical Applications / revista Key Engineering Materials (BDI)*, DOI: 10.4028/p-r405h8 <https://www.scientific.net/KEM.931.55>, **Quan, PH**, Paltanea V.M., Paltanea G., Antoniac I., Nemoianu I.V.,

**3. Review** - *Magnesium-Based Alloys Used in Orthopedic Surgery / revista MATERIALS (Q1)*, -

**[https://pubmed.ncbi.nlm.nih.gov/35161092/#:~:text=Magnesium%20\(Mg\)%2Dbased%20alloys,nondegradable%20metals%20implants%20in%20orthopedics](https://pubmed.ncbi.nlm.nih.gov/35161092/#:~:text=Magnesium%20(Mg)%2Dbased%20alloys,nondegradable%20metals%20implants%20in%20orthopedics)** Antoniac, I; Miculescu, M; Manescu, V; Stere, A; Quan, PH; Paltanea, G; **Robu, A**; Earar, K. Magnesium-Based Alloys Used in Orthopedic Surgery, *Materials*, 2022, 15, 1148, **<https://doi.org/10.3390/ma15031148>**

**4. Article** - *The effects of Machine parameters to surface roughness when cutting WEDM alloy steel by Taguchi method and ANOVA*, **Pham Hong Quan**, pp 35 – 39, Vol. 29.2015, Journal of science & Technology, Vietnam

**5. Article** - *Evaluating the effects of technological parameters of cutting process WEDM on surface roughness using Taguchi's method and ANOVA*, **Pham Hong Quan**, pp 87- 92, Vol. 10.2015, Vietnam mechanical engineering Journal, Vietnam.

**6. Article** - *Design of experiments using Taguchi's method for research the effects of cutting regime on surface roughness molds of die sinking EDM process*, **Pham Hong Quan**, pp 8 – 14, Vol. 8 December 2015, Journal of science and Technology, Vietnam.

### Conferences participations:

1. *Evaluation of release Biodegradability and Corrosion for Biodegradable Magnesium alloys containing Silver*, Iulian Antoniac 1, **Pham Hong Quan 1\***, Izabela Ciuntuc 1, Claudia Milea



- 1, Vicentiu Saceleanu 2, in 7th International Conference on Materials Science and Technologies, November 15th-18th 2018, Bucharest Romania
2. ***Evaluation of release Biodegradability and Corrosion for some Biodegradable Magnesium alloys with Antibacterial Properties after Hydroxyapatite Coatings***, Iulian Antoniac 1, **Pham Hong Quan** 1\*, Izabela Ciuntuc 1, Claudia Milea 1, Simona Cavalu 2, Vicentiu Saceleanu 3, in 8th International Conference Biomaterials, Tissue Engineering & Medivices, September 27th-29th 2018, Cluj-Napoca Romania
3. ***Characterization and biodegradation evaluation of the hydroxyapatite coatings deposited by magnetron sputtering on biodegradable magnesium alloys type Mg-Zn-Zr-Ag***, C. Milea 1, I. Antoniac 1, A. Antinoac 1, E. Ploeanu 1, **P.h Quan** 1, C. Cotrut 1, E. Vasile 1, A. Vladescu 2, V. Saceleanu 3, in 11th International Conference on Materials Science and engineering, Marth 13th-16th 2019, Brasov Romania
4. ***Performing and Characterization of Biodergadable Magnesium Alloys Type Mg-Zn-Zr-Ag Coated with Hydroxiapatite***, Elena Grosu 1, Claudia Milea 1, Aurora Antioniac 1, **Pham Hong Quan** 1, Alina Vladescu 2, Eugeniu Vasile 1, iunian Antoniac1, in Internatinal Conference on Innovative Research, May 16th-17th 2019, Iasi Romania

## List of figures

- Figure 1.1.** Bone structure [1]  
**Figure 1.2** Types of fractures of bones [3]  
**Figure 1.3** Microscopic aspects highlighting the osseointegration of a metallic implant: macroscopic image (a) and microscopic image (b) [5]  
**Figure. 1.4.** Examples of different metallic trauma implants  
**Figure 1.5.** Trauma implants made by stainless steel [11]  
**Figure 1.6.** Application of bioresorbable materials  
**Figure 1.7** Total magnesium consumption in 2021 in the world [17].  
**Figure 1.8.** The main six Mg-based binary alloys for orthopedical applications [4]  
**Figure 1.9.** Methods used for the evaluation of the biodegradable Mg alloys for temporary orthopedic implants.  
**Figure 1.10.** Mg-Zn binary phase diagram [138].  
**Figure 1.11.** Biodegradation mechanism of metals [65]  
**Figure 1.12.** The corrosion mechanisms in Mg-based alloys in SBF solution [68].  
**Figure 1.13** Schematic representation of corrosion types  
**Figure 1.14.** Magnesium pH-potential equilibrium according to Pourbaix (adapted from [76]):  
**Figure 1.15.** Degradation behavior of Mg-based temporary implants in bone fracture healing process, in ideal conditions (adapted after [50]).  
**Figure 1.16.** Correlation between degradation and the mechanical integrity in the healing period of time [80,90,91]  
**Figure 1.17.** Small and large animal models and associated tested geometries.  
**Figure 1.18.** Absorption phenomenon and excretion equilibrium of Mg in the human body system [4].  
**Figure 1.19.** Coatings scheme for biodegradable magnesium alloys [174].  
**Figure 1.20.** Coatings effects on a magnesium alloy  
**Figure 1.21.** Mg alloys with phosphate-based conversion coatings.  
**Figure 3.1.** Ingots of (a) Sample 1 and (b) Sample 2 magnesium alloys  
**Figure 3.2.** Sample 1 and (b) Sample 2 magnesium alloys and the cutting machine (Bernardo MBS 2800G)  
**Figure 3.3.** Experimental samples after cutting  
**Figure 3.4.** Experimental samples after grinding and polishing– sample 1 type  
**Figure 3.5.** Experimental samples after grinding and polishing– sample 2 type  
**Figure 3.6.** Experimental probes for mechanical testing – sample 1 type  
**Figure 3.7.** Experimental probes for mechanical testing – sample 2 type  
**Figure 3.8.** – Samples after the sandblasting process - sample 1  
**Figure 3.9.** – Samples after the sandblasting process – sample 2  
**Figure 3.10** – The samples after the HF treatment – sample 1  
**Figure 3.11** – The samples after the HF treatment – sample 2  
**Figure 3.12** – The samples after the Sandblasting + HF treatment – sample 1  
**Figure 3.13** – The samples after the Sandblasting + HF treatment – sample 2  
**Figure 3.14.** Optical microscope structure  
**Figure 3.15.** Schematic Representation on the Working Principles of X-ray Diffraction  
**Figure 3.16.** Schematic diagram of EDS system  
**Figure 3.17.** Two basic stereo microscope principles: a) the telescope or CMO principle b) the Greenough principle  
**Figure 3.18.** – The samples after Immersion test  
**Figure 4.1.** Area of interest in the Mg-Zn binary diagram [222]

**Figure 4.2.** Detail regarding the eutectic transformation from the Mg-Zn binary diagram [222].

**Figure 4.3.** The optical micrographs corresponding to the type of alloy Mg-Nd-Y-Zn-Zr alloys corresponding to the chemical composition of sample 1

**Figure 4.4.** The optical micrographs corresponding to the type of alloy Mg-Nd-Y-Zn-Zr alloys corresponding to the chemical composition of sample 2

**Figure 4.5.** XRD diffraction patterns on untreated and treated Sample 1 alloys

**Figure 4.6.** XRD diffraction patterns on untreated Sample 2 alloys

**Figure 4.7.** SEM-EDX images obtained after the surface analysis of the untreated Sample 1 alloy, highlighting the compounds at the grain boundary (red) and the surface composition (blue).

**Figure 4.8.** SEM-EDX images obtained after the surface analysis of the untreated Sample 2 alloy, highlighting the compounds at the grain boundary (yellow) and the surface composition (green).

**Figure 4.9.** The contact angles measurements for each type of Sample 1 sample with three liquids (diiodomethane, ethylene glycol and water)

**Figure 4.10.** The contact angles measurements for each type of Sample 2 sample with three liquids (diiodomethane, ethylene glycol and water)

**Figure 4.11** The open circuit potential curves of magnesium alloys: Sample 1

**Figure 4.12** The open circuit potential curves of sample 2 of alloys investigated

**Figure 4.13** The Tafel plots of sample 1 of the alloys investigated

**Figure 4.14** The Tafel plots of sample 3 of the alloys investigated

**Figure 4.15.** Weight loss of untreated and treated Sample 1 and Sample 2 samples after 1, 3, 5, 7 and 14 days of immersion in NaCl solution

**Figure 4.16.** Macroscopic aspect of the untreated alloys investigated of the samples 1 after 1, 3, 5, 7 and 14 days of immersion in sodium chloride solution

**Figure 4.17.** Macroscopic aspect of the untreated alloys investigated of the samples 2 after 1, 3, 5, 7 and 14 days of immersion in sodium chloride solution

**Figure 4.18.** Surface morphologies of the original experimental sample Sample 1 after 5 days of immersion in sodium chloride solution – with the highlighting of the spherical corrosion products

**Figure 4.19.** Surface morphologies of the original experimental sample Sample 1 after 14 days of immersion in sodium chloride solution – with the highlighting of the clusters

**Figure 4.20** Surface morphologies of the original experimental sample Sample 2 after 7 days of immersion in sodium chloride solution – with the highlighting of the corrosion products

**Figure 4.21.** Schematic of tensile test showing elongation of tensile specimen at different strains.

**Figure 4.22** Photos of sample 1 after the tensile test

**Figure 4.23.** Photos of sample 2 after tensile test

**Figure 4.24** The tensile stress-stress diagrams highlighting the mechanical properties of the alloys investigated.

**Figure 4.25** The tensile stress-stress diagrams highlighting the mechanical properties of the alloys investigated.

**Figure 4.26.** SEM images obtained after tensile strength testing for original untreated for bought samples.

**Figure 5.1.** X-ray Diffraction (XRD) diffraction patterns on treated Sample 1 alloys

**Figure 5.2.** X-ray Diffraction (XRD) diffraction patterns on treated Sample 2 alloys

**Figure 5.3.** Sample 1 – SEM images for the original and threated surfaces

**Figure 5.4.** Sample 2 – SEM images for the original and threated surfaces

**Figure 5.5.** The contact angles measurements for samples 1 threated physic-chemical with three liquids (diiodomethane, ethylene glycol and water)

**Figure 5.6.** The contact angles measurements for samples 2 threated physic-chemical with three liquids (diiodomethane, ethylene glycol and water)

**Figure 5.7.** The open circuit potential curves of the sample 1 investigate alloy  
**Figure 5.8.** The open circuit potential curves of the sample 2 investigate alloy  
**Figure 5.9.** The Tafel plots of the sample 1 investigate alloy  
**Figure 5.10.** The Tafel plots of the sample 2 investigate alloy  
**Figure 5.11.** Weight loss of untreated and treated Sample 1 and Sample 2 after 1, 3, 5, 7 and 14 days of immersion in NaCl solution  
**Figure 5.12.** Macroscopic aspect of the experimental samples treated with hydrofluoric acid after 1, 3, 5, 7, and 14 days of immersion in sodium chloride solution  
**Figure 5.13.** Macroscopic aspect of the experimental samples treated with hydrofluoric acid after 1, 3, 5, 7, and 14 days of immersion in sodium chloride solution  
**Figure 5.14.** Macroscopic aspect of the sandblasted experimental samples after 1, 3, 5, 7, and 14 days days of immersion in sodium chloride solution – for sample 1  
**Figure 5.15.** Macroscopic aspect of the sandblasted experimental samples after 1, 3, 5, 7, and 14 days days of immersion in sodium chloride solution – for sample 2  
**Figure 5.16.** Macroscopic aspect of the sandblasted and treated with HF experimental samples 1 after 1, 3, 5, 7, and 14 days of immersion in sodium chloride solution  
**Figure 5.17.** Macroscopic aspect of the sandblasted and treated with HF experimental samples 2 after 1, 3, 5, 7, and 14 days of immersion in sodium chloride solution  
**Figure 5.18.** SEM images aspect of the experimental samples 1 after 5 days of immersion in sodium chloride solution  
**Figure 5.19.** SEM images aspect of the experimental samples 1 after 14 days of immersion in sodium chloride solution  
**Figure 5.20.** SEM images aspect of the experimental samples 2 after 5 days of immersion in sodium chloride solution  
**Figure 5.21.** SEM images aspect of the experimental samples 2 after 14 days of immersion in sodium chloride solution  
**Figure 5.22.** SEM images aspect of the sandblasted with HF-treated samples 1 and 2 after 7 days of immersion in sodium chloride solution

#### **List of tables**

**Table 1.1.** Temporary fixation devices for different fracture types in human and animal models [4].  
**Table 1.2** Classification of biomaterials [1]  
**Table 1.3** Compositions of various grades of stainless steels acceptable as metallic grade surgical steel [12]  
**Table 1.4.** Mechanical properties of biomedical titanium alloys  
**Table 1.5.** Physiological and toxicological characteristics of the impurities in Mg-based alloys [59].  
**Table 1.6.** Physiological and toxicological characteristics of the alloying elements in Mg-based alloys [59].  
**Table 1.7.** Chemical composition of some biodegradable magnesium alloys for medical applications.  
**Table 1.8.** Examples with different animal models and Mg-based implants used in the studies.  
**Table 2.1.** Research methodology. Stages of the experimental program.  
**Table 2.2.** Methods of characterization of the obtained samples  
**Table 3.1.** The chemical compositions of the experimental samples  
**Table 3.2.** Coding of experimental samples  
**Table 3.3.** Methods of characterization of the obtained samples

**Table 4.1.** Contact angle measurements values for sample 1

**Table 4.2.** Contact angle measurements values for sample 2

**Table 4.3.** Main obtained electrochemical parameters

**Table 4.4.** Weight loss measurements values

**Table 5.1.** Contact angle measurements values for samples 1

**Table 5.2.** Contact angle measurements values for samples 2

**Table 5.3.** Main obtained electrochemical parameters

### List of abbreviations

SBF solution – simulated bodily fluid solution

Mg-RE alloys – Magnesium Rare earths alloys

RE - Rare earths

Ca-P - calcium phosphate

HA – hydroxyapatite

HF - hydrofluoric acid

MgF<sub>2</sub> - Magnesium fluoride

DCP – di-calcium phosphate

EDTA - Ethylenediaminetetraacetic acid

PEO = MAO - Plasma electrolytic oxidation

PVD - Physical Vapor Deposition

CPT - Co-precipitation - refers to the simultaneous precipitation of multiple substances that are typically dissolved in solution

LDH coatings - Layered Double Hydroxide coatings

ED - Electrolytic deposition

PLA - Polylactic acid

XRD – X-ray diffraction analysis

EDS – Energy Dispersive Spectroscopy

SEM – Scanning Electron Microscopes

MRI 201S – Sample 1

MRI 202S –Sample 2

SiC - silicon carbide abrasive papers

E<sub>OC</sub> - open circuit potential

E<sub>corr</sub> - corrosion potential

i<sub>corr</sub> - corrosion current density

β<sub>c</sub> - cathodic Tafel slope

β<sub>a</sub> - anodic Tafel slope

SH – sandblasted and treated with HF sample

H – treated with HF sample

S - sandblasted sample

### Bibliography

1. Omema, U.; Khalid, H.; Chaudhry, A.A. Magnesium-Substituted Hydroxyapatite. In *Handbook of Ionic Substituted Hydroxyapatites*; Elsevier, 2020; pp. 197–216.
2. Antoniac, I.; Miculescu, M.; Mănescu, V.; Stere, A.; Quan, P.H.; Păltânea, G.; Robu, A.; Earar, K. Magnesium-Based Alloys Used in Orthopedic Surgery. *Materials* **2022**, *15*, doi:10.3390/ma15031148.

3. Xu, L.; Liu, X.; Sun, K.; Fu, R.; Wang, G. Corrosion Behavior in Magnesium-Based Alloys for Biomedical Applications. *Materials* **2022**, *15*, 2613, doi:10.3390/ma15072613.
4. Chakraborty Banerjee, P.; Al-Saadi, S.; Choudhary, L.; Harandi, S.E.; Singh, R. Magnesium Implants: Prospects and Challenges. *Materials* **2019**, *12*, 136, doi:10.3390/ma12010136.
5. Gu, X.-N.; Li, S.-S.; Li, X.-M.; Fan, Y.-B. Magnesium Based Degradable Biomaterials: A Review. *Front Mater Sci* **2014**, *8*, 200–218, doi:10.1007/s11706-014-0253-9.
6. Esmaily, M.; Svensson, J.E.; Fajardo, S.; Birbilis, N.; Frankel, G.S.; Virtanen, S.; Arrabal, R.; Thomas, S.; Johansson, L.G. Fundamentals and Advances in Magnesium Alloy Corrosion. *Prog Mater Sci* **2017**, *89*, 92–193, doi:10.1016/j.pmatsci.2017.04.011.
7. Hornberger, H.; Virtanen, S.; Boccaccini, A.R. Biomedical Coatings on Magnesium Alloys – A Review. *Acta Biomater* **2012**, *8*, 2442–2455, doi:10.1016/j.actbio.2012.04.012.
8. Antoniac, I.; Miculescu, M.; Mănescu, V.; Stere, A.; Quan, P.H.; Păltânea, G.; Robu, A.; Earar, K. Magnesium-Based Alloys Used in Orthopedic Surgery. *Materials* **2022**, *15*.
9. Quan, P.H.; Antoniac, I.; Miculescu, F.; Antoniac, A.; Manescu, V.; Robu, A.; Bița, A.-I.; Miculescu, M.; Saceleanu, A.; Bodog, A.D.; et al. Fluoride Treatment and In Vitro Corrosion Behavior of Mg-Nd-Y-Zn-Zr Alloys Type. *Materials* **2022**, *15*, doi:10.3390/ma15020566.
10. ASTM G5-14.
11. Shao, G.; Varsani, V.; Fan, Z. Thermodynamic Modelling of the Y–Zn and Mg–Zn–Y Systems. *Calphad* **2006**, *30*, 286–295, doi:10.1016/j.calphad.2006.03.005.
12. <https://www.teachpe.com/anatomy-physiology/structure-of-bones>.
13. <https://www.britannica.com/facts/fracture-of-bone>.
14. <http://michaldrozdowski.pl/biocompatibility-and-osteointegration-of-dental-implants/?lang=en>.
15. <https://compartirmateriales.blogspot.com/2019/04/de-que-material-son-los-tornillos.html>.
16. <https://www.stainless.eu/en/products/cobalt-alloys/>.
17. *MAGNESIUM METAL Defined as Primary Production + Secondary Production from Old Scrap + Imports-Exports + Adjustments for Industry Stock Changes. 3 Source: S&P Global Platts Metals Week. 4 Defined as Imports-Exports + Adjustments for Industry Stock Changes;*
18. Han, H.-S.; Loffredo, S.; Jun, I.; Edwards, J.; Kim, Y.-C.; Seok, H.-K.; Witte, F.; Mantovani, D.; Glyn-Jones, S. Current Status and Outlook on the Clinical Translation of Biodegradable Metals. *Materials Today* **2019**, *23*, 57–71, doi:10.1016/j.mattod.2018.05.018.
19. Xu, L.; Liu, X.; Sun, K.; Fu, R.; Wang, G. Corrosion Behavior in Magnesium-Based Alloys for Biomedical Applications. *Materials* **2022**, *15*, 2613, doi:10.3390/ma15072613.
20. Zheng, Y.F.; Gu, X.N.; Witte, F. Biodegradable Metals. *Materials Science and Engineering: R: Reports* **2014**, *77*, 1–34, doi:10.1016/j.mser.2014.01.001.
21. Hermawan, H. Updates on the Research and Development of Absorbable Metals for Biomedical Applications. *Prog Biomater* **2018**, *7*, 93–110, doi:10.1007/s40204-018-0091-4.
22. Yin, Z.-Z.; Qi, W.-C.; Zeng, R.-C.; Chen, X.-B.; Gu, C.-D.; Guan, S.-K.; Zheng, Y.-F. Advances in Coatings on Biodegradable Magnesium Alloys. *Journal of Magnesium and Alloys* **2020**, *8*, 42–65, doi:10.1016/j.jma.2019.09.008.
23. Wagner, D.C.; Chai, X.; Tang, X.; Kou, S. Liquation Cracking in Arc and Friction-Stir Welding of Mg-Zn Alloys. *Metallurgical and Materials Transactions A* **2015**, *46*, 315–327, doi:10.1007/s11661-014-2606-5.